

Exponential Krylov time integration for modeling multi-frequency optical response with monochromatic sources

M.A. Botchev^{a,b,*}, A.M. Hanse^{c,d}, R. Uppu^e

^a*Keldysh Institute of Applied Mathematics, Russian Academy of Sciences, Miusskaya Sq. 4, 125047 Moscow, Russia*

^b*Skolkovo Institute of Science and Technology, Skolkovo Innovation Center, Bldg 3, 143026 Moscow, Russia*

^c*International School Twente, Het Stedelijk Lyceum, Tiemeister 20, 7541WG Enschede, the Netherlands*

^d*Department of Applied Mathematics and MESA+ Institute for Nanotechnology, University of Twente, P.O. Box 217, 7500 AE Enschede, the Netherlands*

^e*Complex Photonic Systems group (COPS) and MESA+ Institute for Nanotechnology, University of Twente, P.O. Box 217, 7500 AE Enschede, the Netherlands*

Abstract

Light incident on a layer of scattering material such as a piece of sugar or white paper forms a characteristic speckle pattern in transmission and reflection. The information hidden in the correlations of the speckle pattern with varying frequency, polarization and angle of the incident light can be exploited for applications such as biomedical imaging and high-resolution microscopy. Conventional computational models for multi-frequency optical response involve multiple solution runs of Maxwell's equations with monochromatic sources. Exponential Krylov subspace time solvers are promising candidates for improving efficiency of such models, as single monochromatic solution can be reused for the other frequencies without performing full time-domain computations at each frequency. However, we show that the straightforward implementation appears to have serious limitations. We further propose alternative ways for efficient solution through Krylov subspace methods. Our methods are based on two different splittings of the unknown solution into different parts, each of which can be computed efficiently. Experiments demonstrate a significant gain in computation time with respect to the standard solvers.

Keywords: light scattering, mesoscopic optics, disordered media, finite difference time domain (FDTD) methods, Krylov subspace methods, exponential time integration
2008 MSC: 65F60, 65F30, 65N22, 65L05, 35Q61

*Corresponding author. Work of this author is supported by the Russian Science Foundation Grant 17-11-01376.

Email addresses: botchev@kiam.ru (M.A. Botchev), abelhanse@gmail.com (A.M. Hanse), r.uppu@utwente.nl (R. Uppu)

1. Introduction

Modeling of light propagation is an important and ever-growing research area [12, 47]. Understanding the propagation of light in a scattering medium has widespread applications such as real-time medical imaging, spectrometry, and quantum security [4, 35, 55, 42, 26]. A complex scattering medium comprises of a regular or an irregular spatial arrangement of inhomogeneities in refractive index. While the former are complex fabricated structures known as photonic crystals, we experience the latter in common materials such as skin, sugar, and white paint. Light propagating through a layer of such random scattering media undergoes multiple scattering off the inhomogeneities resulting in a complex interference pattern, called the speckle pattern [2]. The seemingly random speckle patterns possess rich correlations which depend on parameters such as the frequency, angle of incidence and spectral content of the propagating light [22, 52, 16, 39]. These correlations help in revealing fundamental light transport properties of the medium which are instrumental for different applications.

An important modeling approach to analyze frequency correlations of speckle pattern is through the so-called broadband pulse excitation (BPE). Mathematically, this modeling approach solves the time-dependent Maxwell equations with a source function (representing the incident light) taken as a short Gaussian pulse in time. The frequency bandwidth of the pulse is inversely related to the temporal width of the pulse, therefore shorter the pulse, broader the frequency bandwidth. The speckle patterns at different frequencies can then be obtained by taking a Fourier-transform of the optical response (which is the resulting electromagnetic field after time T of computation when the incident pulse has decayed). A drawback of the BPE approach is that the accuracy of the results is subject to the time-window of computation, which is necessarily short for broadband light. The separation of single frequency response from the total response will be compromised by the frequency resolution of Fourier-transformed fields. In fact, the BPE can be seen a compromise between accuracy (increasing if the frequency bandwidth gets narrower) and efficiency (increasing if the frequency bandwidth gets broader). To avoid this potential loss in accuracy in BPE simulations or to verify the BPE results, time-domain computations with pulses of a single frequency have to be carried out.

This paper explores a way to utilize the single frequency time-domain computations for efficiently computing the multi-frequency response with the help of the Krylov subspace exponential time integration. These methods are based on a projection (onto the Krylov subspace) which is carried out independently of the frequency in the source term. Hence, the same projection is used to obtain a small-dimensional projected problem for optical response at a different frequency. Therefore, the Krylov subspace methods should be computationally more efficient in comparison to multiple single frequency computations. Moreover, the projection methods achieve the computational efficiency without compromising the accuracy unlike BPE.

Exponential time integration has received much attention in the recent decades. These methods involve actions of the matrix functions, such as matrix exponential and matrix cosine. The efficiency of the methods depends on their implementation. For large matrices, methods to compute matrix function actions on a vector include Krylov sub-

space methods (based on Lanczos or Arnoldi processes), Chebyshev polynomials (primarily for Hermitian matrices), and scaling and squaring with Padé or Taylor approximations and some other methods [48, 15, 45, 10, 3]. In this paper we use Krylov subspace methods for computing the matrix exponential actions on vectors; these methods are suitable for non-Hermitian matrices, have been significantly improved recently [19, 38, 50, 27] and successfully applied to solving time-dependent Maxwell and wave equations [17, 5, 32, 7].

We discuss implementation of our Krylov subspace exponential integration method in detail in Section 3.2. Unfortunately, this approach appears to have its limitations. To circumvent the limitations, we also design other solution strategies with the Krylov subspace exponential time integration. A key idea which leads to a very competitive method is to utilize the time asymptotic behavior of the solution in the Krylov subspace framework. Another approach we develop is based on a splitting of the problem into a number of easier to solve homogeneous problems and nonhomogeneous problems which appear to be identical due to the periodicity of the source term.

The rest of this article is organized as follows. A precise formulation of the problem is discussed in Section 2. The existing and proposed solution methods are presented in Section 3. We discuss numerical experiments in Section 4, which is followed by conclusions.

2. Problem formulation and current solution methods

2.1. Modeling multi-frequency optical response in scattering medium

We consider the scattering material to compose of infinitely long cylinders of radius r which are randomly spaced with the minimum distance $d = 2r$. The symmetry of the scattering medium along z -axis (i.e., along the longitudinal axis of the cylinders) can be used to solve a two-dimensional computational model. The scattering material extends from $x = a_x$ to $x = b_x$ with perfect electric conductors at $y = a_y$ to $y = b_y$. The incident light originates from a point electric dipole. The propagation of light is modeled by solving time-dependent Maxwell equations using finite-difference time-domain methods. After a relatively long time, the light transmits through the scattering layer, where its intensity eventually approaches a time asymptotic regime, i.e., becomes a time periodic function. The result of the computations is the intensity speckle pattern formed in the transmission of the scattering layer. The aim of the modeling is to study correlations of the speckle patterns depending on the frequency ω (to be precisely defined later in this section) of the incident light.

To numerically solve the Maxwell equations, we first make the equations dimensionless. We follow the standard dimensionless procedure as described, e.g., in [7]. In the two-dimensional computational model, the unknown field components are $H_x(x, y)$, $H_y(x, y)$ (magnetic field) and $E_z(x, y)$ (electric field) as the incident light originates from a point electric dipole. Although the problem is two-dimensional, the size of the discretized problem has to be large (in this paper up to $\approx 5 \cdot 10^6$ degrees of freedom) to resolve the inhomogeneities in the scattering medium. More precisely, we solve the two-dimensional Maxwell equations in a domain $(x, y) \in [a_x, b_x] \times [a_y, b_y]$ with perfectly

electric conducting boundary conditions ($E_z = 0$) at the y -boundaries and nonreflecting boundary conditions at the x -boundaries. The nonreflecting boundary conditions are implemented as the perfectly matched layers (PMLs) and the resulting dimensionless Maxwell equations read:

$$\begin{aligned}\frac{\partial H_x}{\partial t} &= -\frac{1}{\mu_r} \frac{\partial E_z}{\partial y}, \\ \frac{\partial H_y}{\partial t} &= \frac{1}{\mu_r} \frac{\partial E_z}{\partial x} - \sigma_x H_y, \\ \frac{\partial E_z}{\partial t} &= \frac{1}{\epsilon_r} \left(\frac{\partial H_y}{\partial x} - \frac{\partial H_x}{\partial y} - J_z \right) - \sigma_x E_z + P, \\ \frac{\partial P}{\partial t} &= -\frac{\sigma_x}{\epsilon_r} \frac{\partial H_x}{\partial y},\end{aligned}\tag{1}$$

where H_x , H_y , E_z are the unknown field components, μ_r and ϵ_r are the relative permeability and relative permittivity, respectively, and $P = P(x, y, t)$ is an auxiliary PML variable. The details of the derivation of the PML boundary conditions can be found in [34, 29]. In our case $\mu_r \equiv 1$ throughout the domain of interest and $\epsilon_r(x, y)$ is a piecewise constant function representing the inhomogeneities in the scattering medium. Furthermore, the damping terms $\sigma_x H_y$ (which is nonphysical) and $\sigma_x E_z$ are due to the PML boundary conditions. σ_x is nonzero only in the so-called PML regions (situated just outside of the domain $[a_x, b_x] \times [a_y, b_y]$ along the x -boundaries, where the field is damped). Finally,

$$J_z(x, y, t) = \alpha(t)J(x, y), \quad \alpha(t) = \sin(2\pi\omega t)\tag{2}$$

is the source term, where $J(x, y)$ is nonzero only at the boundary $x = a_x$. At the initial time $t = 0$ initial conditions

$$H_x = 0, \quad H_y = 0, \quad E_z = 0, \quad P = 0\tag{3}$$

are imposed.

To solve (1) with additional PML equations numerically, we follow the method of lines approach, i.e., we first discretize the equations in space. In this paper, we use the standard finite-difference Yee space discretization, where the electric field values are situated at the grid vortices and the magnetic field values at the centers of the grid edges. Alternatively, any other suitable space discretization can be used for this problem, for instance, vector Nédélec finite elements (see e.g. [9]) or discontinuous Galerkin finite elements (see e.g. [44]). The space discretization then results in a system of ordinary differential equations (ODEs)

$$\begin{cases} y'(t) = -Ay(t) + \alpha(t)g, \\ y(0) = v, \end{cases} \quad y = \begin{bmatrix} \bar{H}_x \\ \bar{H}_y \\ \bar{E}_z \\ \bar{P} \end{bmatrix}, \quad A = \begin{bmatrix} \hat{A} & B_1^T \\ -B_2 & 0 \end{bmatrix}, \quad 0 < t < T,\tag{4}$$

where $\bar{H}_x, \bar{H}_y, \bar{E}_z, \bar{P}$ are the grid values of the unknown fields and the auxiliary PML variable and \hat{A} is the Maxwell operator matrix corresponding to the space discretized equations (1),

$$\hat{A} = \begin{bmatrix} M_\mu^{-1} & 0 \\ 0 & M_\epsilon^{-1} \end{bmatrix} \begin{bmatrix} M_{\sigma_x} & K \\ -K^T & M_{\sigma_x} \end{bmatrix}.$$

Here $M_{\epsilon, \mu, \sigma_x}$ are diagonal matrices containing the grid values of ϵ, μ, σ_x , respectively, and K is a discretized two-dimensional curl operator. In our problem, due to (3), the initial value v is zero but, for the purpose of presentation, we prefer to write v there instead of a zero vector.

In the remainder of the paper we denote the total dimension of the problem (4) by n , i.e., $A \in \mathbb{R}^{n \times n}$. It can be shown that the eigenvalues of \hat{A} have nonnegative real part, see e.g. [9]. We assume that the property holds for the matrix A , as is shown numerically in [7].

3. Solution methods

3.1. Standard finite difference time domain methods (FDTD)

A well established and widely used class of methods to model electromagnetic scattering (4) is the finite-difference time-domain methods [47]. In the framework of the method of lines, these methods essentially imply a finite difference approximation in space (often employing the Yee cell [54]) and a subsequent application of a time integration method. The celebrated Yee scheme is an example of this approach, where the time discretization is based on a second order symplectic composition scheme [9]. This compact, energy preserving time integration scheme can be viewed as a combination of the staggered leap-frog scheme for the wave terms (represented by the matrices K and K^T in (4)) and the implicit trapezoidal scheme (ITR) for the damping terms M_{σ_x} . However, when applied to the problems with PML boundary conditions, the method loses its clarity and represents essentially an ad-hoc splitting implicit-explicit scheme where the stiff PML terms are treated implicitly.

Our problem is two-dimensional and, hence, although large, can be efficiently treated by fully implicit FDTD schemes. The arising linear systems can then be solved by sparse direct solvers, which have been significantly improved last decades [14, 13, 20]. In addition, an employment of an implicit scheme is simple and removes the necessity to handle the PML terms in a special way. An implicit scheme which is very suitable for the Maxwell equations is the classical ITR (also known as the Crank–Nicolson scheme). The scheme is second-order accurate, does not introduce artificial damping and preserves energy [53]. Therefore, in this paper we choose ITR to be the reference FDTD method. For our problem (4) it reads

$$\frac{y^{k+1} - y^k}{\tau} = -\frac{1}{2}Ay^k - \frac{1}{2}Ay^{k+1} + \frac{1}{2}\alpha^k g + \frac{1}{2}\alpha^{k+1}g,$$

where $\tau > 0$ is the time step size and the superindex k indicates the time step number. At every time step a linear system with a matrix $I + \frac{1}{2}\tau A$ has to be solved.

3.2. Krylov subspace methods, basic facts

Let $y_0(t)$ be an approximation (initial guess) to the solution $y(t)$ of (4). Let us define the error (unknown in practice) and the residual of $y_0(t)$ as (cf. [11, 18, 36])

$$\begin{aligned}\varepsilon_0(t) &:= y(t) - y_0(t), \\ r_0(t) &:= -Ay_0(t) - y_0'(t) + \alpha(t)g.\end{aligned}\tag{5}$$

We assume that the residual $r_0(t)$ of the initial guess $y_0(t)$ is known. This can be achieved, for instance, by taking $y_0(t)$ to be a constant function equal to the initial value v :

$$r_0(t) = -Av + \alpha(t)g = \alpha(t)g,\tag{6}$$

where the last step obviously holds only if $v = 0$. Note that the initial residual turns out to be a time dependent scalar function times a constant vector. Furthermore, if $y_0(t)$ satisfies the initial condition $y_0(0) = v$, we have

$$\varepsilon_0'(t) = -A\varepsilon_0 + r_0(t), \quad \varepsilon_0(0) = 0.\tag{7}$$

Starting with $y_0(t)$, Krylov subspace methods obtain a better solution $y_m(t)$ by solving (7) approximately:

$$y_m(t) = y_0(t) + \tilde{\varepsilon}_0(t).\tag{8}$$

Here $\tilde{\varepsilon}_0(t) \approx \varepsilon_0(t)$ is the approximate solution of (7) obtained by m Krylov steps. In this paper we use a regular Krylov subspace method [43, 51] as well as a rational shift-and-invert (SaI) Krylov subspace method [38, 50]. The two methods employ the Arnoldi process to produce, after m steps, upper-Hessenberg matrices $\underline{H}_m, \tilde{\underline{H}}_m$, respectively, and an $n \times m$ matrix

$$V_m = [v_1 \quad \dots \quad v_m] \in \mathbb{R}^{n \times m},$$

such that $V_m^* V_m$ is the $m \times m$ identity matrix and

$$\begin{aligned}\text{either } AV_m &= V_{m+1} \underline{H}_m \quad (\text{for regular Krylov method}), \\ \text{or } (I + \gamma A)^{-1} V_m &= V_{m+1} \tilde{\underline{H}}_m \quad (\text{for SaI Krylov method}).\end{aligned}\tag{9}$$

Here $\gamma > 0$ is a parameter whose choice is discussed later. Note that for simplicity of presentation we slightly abuse notation in these last two relations: the matrix V_{m+1} produced by the regular Krylov method and appearing in the former relation is different from V_{m+1} produced by the SaI Krylov method and appearing in the latter relation. Precise definition of the Arnoldi process is not given here as it can be found in many books, e.g., in [43, Algorithm 6.1] or [51, Figure 3.1].

If the regular Krylov method is used, the columns of the matrix V_m span the Krylov subspace $\mathcal{K}_m(A, g) \equiv \text{span}(g, Ag, A^2g, \dots, A^{m-1}g)$, i.e.,

$$\text{span}(v_1, \dots, v_m) = \mathcal{K}_m(A, g), \quad v_1 = g/\|g\|\tag{10}$$

with v_1 being the normalized stationary part of the initial residual (6). For the SaI method, the relations above hold with A replaced by $(I + \gamma A)^{-1}$. The SaI transformation

results in a better approximation in the Krylov subspace of the eigenmodes corresponding to the small in modulus eigenvalues [38, 50] and, hence, is favorable for solving the time dependent problem (7). Indeed, for some classes of the discretized differential operators A , such as the discretizations of parabolic PDEs with a numerical range along the positive real axis, one can show that the convergence of the SaI methods is mesh independent [50, 25]. Although these results can not be extended to wave-type equations in a straightforward manner, a mesh independent convergence is observed in practice for the Maxwell equations with damping in [7].

For the SaI Krylov method we define the matrix H_m as the inverse shift-and-invert transformation:

$$H_m = \frac{1}{\gamma}(\tilde{H}_m^{-1} - I). \quad (11)$$

The approximate Krylov solution of the correction system (7) can then be written for both Krylov methods as

$$\tilde{\varepsilon}_0(t) = V_m u(t), \quad \begin{cases} u'(t) = -H_m u(t) + \alpha(t)\beta e_1, \\ u(0) = 0, \end{cases} \quad (12)$$

where $e_1 = [1, 0, \dots, 0]^T \in \mathbb{R}^m$, $\beta = \|g\|$ and the ODE system in $u(t)$ is merely a Galerkin projection of (7) onto the Krylov subspace.

The two relations in (9) are called Arnoldi decompositions. It is convenient to use them after re-writing in an equivalent form

$$AV_m = V_m H_m + R_m, \quad (13)$$

$$R_m = \begin{cases} h_{m+1,m} v_{m+1} e_m^T & \text{(for regular Krylov method),} \\ -\frac{h_{m+1,m}}{\gamma} (I + \gamma A) v_{m+1} e_m^T \tilde{H}_m^{-1} & \text{(for SaI Krylov method),} \end{cases}$$

where $e_m = [0, \dots, 0, 1]^T \in \mathbb{R}^m$. This last form of the Arnoldi decompositions emphasizes the fact that the Krylov subspace can be seen, if R_m is small in norm, as an approximate invariant subspace of A .

In both regular and SaI Krylov subspace methods, we control the number of Krylov iterative steps m (which is also the dimension of the Krylov subspace) by checking the residual $r_m(t) = -y'_m(t) - Ay_m(t) + \alpha(t)g$ of the approximation $y_m(t)$ in (8). As stated in [11, 18, 8], the residual $r_m(t)$ can easily be computed as follows.

Lemma 1. [8] *In the regular and SaI Krylov subspace methods (7)–(12) the residual $r_m(t) = -y'_m(t) - Ay_m(t) + \alpha(t)g$ of the approximate solution $y_m(t)$ to system (4) satisfies*

$$r_m(t) = \begin{cases} -h_{m+1,m} e_m^T u(t) v_{m+1} & \text{(for regular Krylov method),} \\ \frac{h_{m+1,m}}{\gamma} e_m^T \tilde{H}_m^{-1} u(t) (I + \gamma A) v_{m+1} & \text{(for SaI Krylov method).} \end{cases} \quad (14)$$

Proof. For a detailed proof and discussion we refer to [8]. However, the problem considered there is slightly different than (4); it is of the form (4) with $g = 0$ and $v \neq 0$.

Therefore, for completeness of the presentation we give a short proof of (14) here. Based on (7),(8), we see that

$$r_m(t) = -y'_m(t) - Ay_m(t) + \alpha(t)g = -\tilde{\varepsilon}'_0(t) - A\tilde{\varepsilon}_0(t) + r_0(t).$$

Substituting $\tilde{\varepsilon}_0 = V_m u(t)$ into this relation using the Arnoldi decomposition (13), we obtain

$$r_m(t) = V_m(-u'(t) - H_m u(t) + \alpha(t)\beta e_1) + R_m u(t) = R_m u(t).$$

□

The methods presented in this subsection up to this point are well known, see e.g. [11, 18, 8]. A first, rather simple but, nevertheless, important conclusion which can be drawn from the presentation is as follows.

Corollary 1. *The regular and SaI Krylov subspace methods (7)–(12) for solving the multi-frequency optical response problem (4) are fully independent of the source time component $\alpha(t)$.*

In other words, if the problem (4) has to be solved for many different $\alpha(t)$, the matrices V_m and either \underline{H}_m or \tilde{H}_m can be computed once and used for all $\alpha(t)$. Only the small projected problem (12) has to be solved for each new $\alpha(t)$ again.

Proof. It is enough to note that by construction the Krylov subspace matrices V_m , \underline{H}_m and \tilde{H}_m do not depend on $\alpha(t)$. □

Corollary 1 allows to significantly save computational work when solving (4) numerically. However, for this problem we can expect that the Krylov methods in the current form will not be efficient. This is because the required simulation time T is very large (typically, several hundred time periods of $\alpha(t)$), so that the Krylov dimension m can become prohibitively large in practice. This effect should be expected to be more pronounced for the regular Krylov method, as the SaI method is typically efficient in the sense that the Krylov dimension required for its convergence is often bounded. Nevertheless, the bad expectations are confirmed in the numerical experiments for both regular and SaI Krylov methods. Therefore, in the next section we discuss ways to restart the Krylov subspace methods.

3.3. Krylov subspace methods with restarting

A very large Krylov dimension m slows down the Krylov method as $m+1$ basis vectors v_1, \dots, v_{m+1} have to be stored and every new basis vector has to be orthogonalized with respect to all previous vectors. Typical approaches to cope with the slowing down in time integration problems are restarting in time and restarting in Krylov dimension. In the first approach, the time interval of interest $[0, T]$ is divided in a number of shorter time intervals, where the problem (4) is solved subsequently. This approach is used, for instance, in the elegant EXPOKIT code [46].

If we implement the restarting-in-time approach in our setting with many different $\alpha(t)$, we see that the initial value vector v is not zero in the second and subsequent

time subintervals. For this reason the initial residual is no longer of the form scalar function times a constant vector (cf. (6)). Instead, the residual can be shown to be of the form $Up(t)$ where $U \in \mathbb{R}^{n \times 2}$, $p : \mathbb{R} \rightarrow \mathbb{R}^2$. For such problems, exponential block Krylov methods [6, 23] can be applied. With this method, it is also possible to solve problems (4) simultaneously for different $\alpha(t)$. The idea is then to represent the residuals corresponding to all different $\alpha(t)$ in one common expression $Up(t)$, where the number of columns k in U can be hopefully kept restricted using the truncated SVD (singular value decomposition). This approach is described in detail in [29]. Numerical results presented there show this approach inefficient due the growth of k .

Another way to keep the Krylov dimension m restricted is restarting in Krylov dimension. A number of strategies for Krylov dimension restarting are developed [49, 1, 21, 40, 8, 28]. Here we consider the residual based restarting [8], which is slightly different from the approach [40] demonstrated to work successfully for solving Maxwell's equations [7].

This restarting approach is based on the observation that the residual in the Krylov method preserves the form (6) of the initial residual $r_0(t)$. Indeed, relation (14) shows that $r_m(t) = \hat{\alpha}(t)\hat{g}$ with

$$\begin{aligned} \hat{\alpha}(t) &= -h_{m+1,m}e_m^T u(t), \quad \hat{g} = v_{m+1} \quad (\text{for regular Krylov method}), \\ \hat{\alpha}(t) &= \frac{h_{m+1,m}}{\gamma} e_m^T \tilde{H}_m^{-1} u(t), \quad \hat{g} = (I + \gamma A)v_{m+1} \quad (\text{for SaI Krylov method}). \end{aligned}$$

Hence, to restart after making m Krylov steps, we carry the update (8), set

$$y_0(t) := y_m(t), \quad r_0(t) := r_m(t) = \hat{\alpha}(t)\hat{g}, \quad (15)$$

discard the computed matrices V_{m+1} , \underline{H}_m (or \tilde{H}_m) and start the Arnoldi process again, with the first Krylov basis vector $v_1 = \hat{g}/\|\hat{g}\|$. The method then proceeds as given by relations (7)–(12), with $\alpha(t)$ and g replaced by $\hat{\alpha}(t)$ and \hat{g} , respectively. After making another m Krylov steps, we can restart again. The following result holds.

Corollary 2. *The restarted regular and SaI Krylov subspace methods (7)–(12),(15) for solving the multi-frequency optical response problem (4) are fully independent of the source time component $\alpha(t)$.*

In other words, if the problem (4) has to be solved for many different $\alpha(t)$, the matrices V_m and either \underline{H}_m or \tilde{H}_m can be computed, at each restart, once and used for all $\alpha(t)$. Only the small projected problem (12) has to be solved, at each restart and for each new $\alpha(t)$, again.

Proof. Observe that, as Corollary 1 states, the vector v_{m+1} in both the regular and SaI Krylov methods is independent of $\alpha(t)$. Hence, so is the vector \hat{g} . Therefore, the second restart starts with $r_0(t) := \hat{\alpha}(t)\hat{g}$, where only $\hat{\alpha}(t)$ depends on $\alpha(t)$. \square

Note that we have to implement this restarting algorithm in such a way that the first restart is made for all the functions $\alpha(t)$, then the second restart for all the functions

- (0) Set $y(T) := 0$.
- (1) Carry out m steps of the Arnoldi algorithm, compute the matrices V_{m+1} and H_m (as given by (11)).
- (2) For each frequency ω :
 - (a) solve the projected problem (12);
 - (b) sample for $t \in [0, T]$ and store $\alpha(t) := \frac{h_{m+1,m}}{\gamma} e_m^T \tilde{H}_m^{-1} u(t)$.
 - (c) stop computations for ω values for which the residual norm $|\alpha(t)| \|(I + \gamma A)v_{m+1}\|$ is small enough.
- (3) Carry out the update (8): $y(T) := y(T) + V_m u(T)$, set $g := (I + \gamma A)v_{m+1}$. Go to step (1).

Figure 1: Restarted Krylov subspace method (7)–(12),(15) for solving (4) for different frequencies ω in the source term $g = \alpha(t)g$. The algorithm is given for the SaI variant of the method.

$\hat{\alpha}(t)$, etc. Otherwise (i.e., if first all the restarts were made for the first $\alpha(t)$, then all the restarts for the second $\alpha(t)$, etc.), we would need to keep all Krylov bases from all the restarts. The algorithm involves sampling and storing, for each $\alpha(t)$, the scalar functions $\hat{\alpha}(t)$ at the end of each restart. We outline the algorithm in Figure 1.

3.4. Using the periodicity of the source function

In this section we discuss two ways to make the numerical solution of (4) more efficient by exploiting the time periodicity of the source function $\alpha(t)g$.

3.4.1. Krylov subspace methods with asymptotic correction

Recall that the eigenvalues of A have nonnegative real part and the time interval of interest $[0, T]$ is large in the sense that the output light has reached a time-periodic “steady” state at time T . Therefore, we may hope to improve the Krylov subspace approximations by splitting off this time-periodic part of the solution.

Corollary 3. *The solution $y(t)$ to the problem (4) can be written as*

$$y(t) = \tilde{y}(t) - \hat{y}(t), \quad \tilde{y}(t) = \text{Im}(e^{i2\pi\omega t} z_{\text{stat}}), \quad \hat{y}(t) = e^{-tA} \text{Im} z_{\text{stat}}, \quad (16)$$

where $z_{\text{stat}} = (A + i2\pi\omega I)^{-1}g$ and $\text{Im} z$ denotes the imaginary part of a vector $z \in \mathbb{C}^n$.

Proof. Since the source term is $\alpha(t)g$, with $\alpha(t) = \sin(2\pi\omega t)$ (cf. (4),(2)), the variation of constants formula (see e.g. [33]) allows us to write the exact solution of (4) as

$$y(t) = \underbrace{e^{-tA}v}_{=0} + \int_0^t e^{(s-t)A} \sin(2\pi\omega s)g ds,$$

where the first term drops out because $v = 0$, cf. (3). Let us consider a function

$$z(t) = \int_0^t e^{(s-t)A} e^{i2\pi\omega s} g ds, \quad i^2 = -1,$$

introduced in such a way that $y(t) = \text{Im } z(t)$. This function can be brought to the form

$$\begin{aligned} z(t) &= e^{-tA} \left[\int_0^t e^{s(A+i2\pi\omega I)} ds \right] g = e^{-tA} (A + i2\pi\omega I)^{-1} \left[e^{s(A+i2\pi\omega I)} \right] \Big|_0^t g = \\ &= e^{-tA} (A + i2\pi\omega I)^{-1} \left[e^{t(A+i2\pi\omega I)} - I \right] g = e^{-tA} \left[e^{t(A+i2\pi\omega I)} - I \right] (A + i2\pi\omega I)^{-1} g = \\ &= \left[e^{i2\pi\omega t} - e^{-tA} \right] (A + i2\pi\omega I)^{-1} g = e^{i2\pi\omega t} z_{\text{stat}} - e^{-tA} z_{\text{stat}}. \end{aligned}$$

Hence, we arrive at (16). \square

Note that the first term $\tilde{y}(t)$ in (16) can be identified as the time-periodic part of the solution, while the second one $\hat{y}(t)$ solves a homogeneous initial-value problem

$$\hat{y}(t)' = -A\hat{y}, \quad \hat{y}(0) = \text{Im } z_{\text{stat}}. \quad (17)$$

Furthermore, we note that $\tilde{y}(t)$ is easy to compute and that solving the homogeneous problem (17) is in general an easier task than solving an initial value problem for the inhomogeneous ODE system (4). Indeed, the former problem is equivalent to evaluating the matrix exponential action which is, in general, cheaper than solving an ODE system [37]. This is why evaluating $y := e^A b$ for a given vector b is often a subtask in modern time integrators [31]. Moreover, the Krylov subspace methods are known to work well for problems of the type (17), and this has been used in the literature, see e.g. [24].

Another argument in favor of solving (4) by applying the splitting (16) is that we hope that $\hat{y}(t)$ should decay asymptotically and, hence, the solution $y(t)$ for large times should be well approximated by $\tilde{y}(t)$. This hope is confirmed in practice (see Section 4). The Krylov subspace method applied to solve (17) can easily be restarted in time and at every restart the norm of the initial value vector is expected to be smaller. Hence, the residual should be smaller and the Krylov subspace methods require less steps to converge.

To get the solutions for the other $\alpha(t)$ we first note that z_{stat} can be found simultaneously for many frequencies ω , see e.g. [29, Section 4.3.1]. We do not discuss this further in this paper because, as compared to other costs, solving a system for z_{stat} is very cheap anyway. Furthermore, assume a solution $\hat{y}_\omega(t)$ is found for a certain frequency ω . Usually, a certain frequency range should be scanned which means that the next frequency of interest ω_{next} is rather close to ω . We first compute $\tilde{y}(t)$ for the new value ω_{next} . Note that we can find $\hat{y}_{\omega_{\text{next}}}(t)$ as $\hat{y}_{\omega_{\text{next}}}(t) = \hat{y}_\omega(t) + w(t)$, where $w(t)$ solves the problem

$$w'(t) = -Aw(t), \quad w(0) = \hat{y}_{\omega_{\text{next}}}(0) - \hat{y}_\omega(0). \quad (18)$$

The Krylov subspace methods applied to this problem is likely to require less iterations than for solving (17) provided that $\|\hat{y}_{\omega_{\text{next}}}(0) - \hat{y}_\omega(0)\| < \|\hat{y}_{\omega_{\text{next}}}(0)\|$.

The algorithm for the Krylov subspace method with asymptotic splitting is outlined in Figure 2. It is important to note that solution of the homogeneous ODE systems (17) and (18) at steps 2 and 4, respectively, can be carried out with any restarting in time and in Krylov dimension. This freedom is used by us to obtain an efficient time integrator in Section 4.

For $\omega = \omega_1$:

1. Compute $z_{\text{stat}}, \tilde{y}(T)$ as given by (16).
2. Solve (17), find $\hat{y}(t)$.
3. Store $\hat{y}_\omega(0) := \text{Im } z_{\text{stat}}$ and $\hat{y}_\omega(T) := \hat{y}(T)$.
Compute the solution $y(T) = \tilde{y}(T) - \hat{y}(T)$.

For $\omega_{\text{next}} = \omega_2, \omega_3, \dots$:

4. Compute $z_{\text{stat}}, \tilde{y}(T)$ as given by (16), set $\hat{y}_{\omega_{\text{next}}}(0) := \text{Im } z_{\text{stat}}$.
5. Solve (18), find $w(T)$, set $\hat{y}_{\omega_{\text{next}}}(T) := \hat{y}_\omega(T) + w(T)$.
6. Update $\hat{y}_\omega(0) := \hat{y}_{\omega_{\text{next}}}(0)$ and $\hat{y}_\omega(T) := \hat{y}_{\omega_{\text{next}}}(T)$.
Compute the solution $y(T) = \tilde{y}(T) - \hat{y}_{\omega_{\text{next}}}(T)$.

Figure 2: Krylov subspace method based on the asymptotic splitting (16)

3.4.2. Splitting off the source term

The second approach we consider here to exploit the time periodicity of the source function $\alpha(t)g$ in (4) is as follows. We solve the problem (4) successfully on subintervals $[0, \Delta T], [\Delta T, 2\Delta T], \dots$ (in other words, we apply restarting in time). To solve (4) on each subinterval $[(k-1)\Delta T, k\Delta T]$, $k = 1, 2, \dots$, we split the problem into two subproblems:

$$\begin{cases} w'_1(t) = -Aw_1, \\ w_1(0) = y((k-1)\Delta T), \end{cases} \quad \begin{cases} w'_2(t) = -Aw_2 + \alpha(t)g, \\ w_2(0) = 0, \end{cases} \quad (19)$$

so that the solution for $t = k\Delta T$ is determined as $y(k\Delta T) = w_1(k\Delta T) + w_2(k\Delta T)$. Note that the second problem has the same solution for every subinterval if $\alpha(t)$ is periodic (which is the case for our problem) and we choose ΔT to be a multiple the time period. Thus the problem for $w_2(t)$ has to be solved for the first subinterval only. For the other subintervals, it suffices only to solve the problem for $w_1(t)$. This approach seems profitable because we again only have to solve a homogeneous problem, i.e., the matrix exponential action has to be computed.

4. Numerical experiments

4.1. Test problem and implementation details

Here we briefly discuss some implementation aspects important for successful application of Krylov subspace methods. In all the experiments we use the SaI version of the Krylov subspace method. The regular Krylov subspace method appears to be inefficient for this problem as too many Krylov iterations are needed for its convergence.

All the numerical experiments presented in this paper are carried out in Matlab on Linux PC with 8 CPUs and 32 Gb of memory. To solve the linear systems with the matrices $(I + \frac{\tau}{2}A)^{-1}$ in the ITR scheme and $(I + \gamma A)^{-1}$ in the SaI Krylov method, Matlab's sparse direct LU factorization (based on the UMFPACK [13]) is used. The factorization can be carried out efficiently because the problem is two-dimensional. The

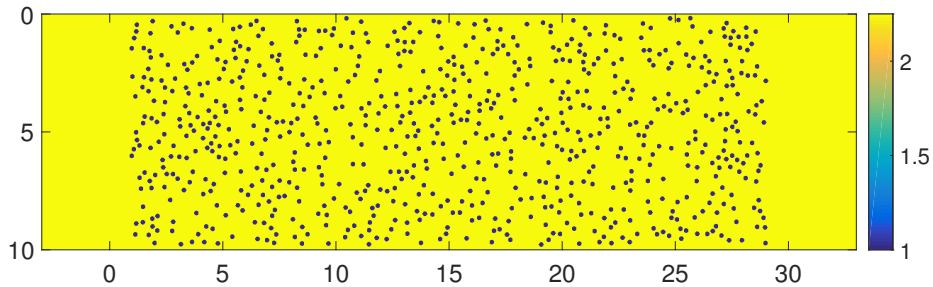


Figure 3: The spatial domain is a waveguide with 750 randomly positioned infinite cylinders

factorization is computed once and used every time the action of the inverse matrices is needed.

We consider the test case where the domain is

$$(x, y) \in [-3, 33] \times [0, 10],$$

and at $y = 0$ and $y = 10$ the perfectly conducting boundary conditions are posed. At $x = 0$ and $x = 30$ the PML boundary conditions are posed, with the PML regions being $x \in [-3, -2]$ and $x \in [32, 33]$. The values of σ_x grow in the PML regions from 0 to $\sigma_{\max} = 20$ quadratically. The final time is set to be $T = 500$.

The region $[0, 30] \times [0, 10]$ contains 750 cylinders of radius 0.1 which are scattered randomly with a minimum distance 0.2 to the domain boundaries and 0.25 from each other. The electric permittivity values are $\epsilon_r = 1$ inside the cylinders and $\epsilon_r = 2.25$ in the rest of the domain (see Figure 3).

The vector g in the source function $\alpha(t)g$ is zero everywhere in the domain except at the line $x = -2$, $y \in [0, 10]$ where it is 1 for $y \in [1, 9]$ and it decays linearly from 1 to 0 for $y \in [0, 1]$ and $y \in [9, 10]$. The time component $\alpha(t)$ of the source function is defined as $\alpha(t) = \sin 2\pi\omega t$ with $\omega \in [0.85, 1.15]$.

The highest resolution which can be used for this domain size is 64 grid points per unit length (4 498 307 , which means that every cylinder is represented by approximately 12×12 grid points. Although this rather rough resolution is sufficient for simulation purposes, to have consistent results for all mesh resolutions we regularize the values of ϵ_r by applying a standard homogenization procedure as follows. Let $(\epsilon_r^0)_{i,j}$ represent the original piecewise constant values of ϵ_r at the mesh points (i, j) for the mesh resolution 256 points per unit length (this resolution is too high to be used for the whole simulation). Then, we update

$$(\epsilon_r^{k+1})_{i,j} = \frac{1}{2}(\epsilon_r^k)_{i,j} + \frac{1}{2} \frac{(\epsilon_r^k)_{i-1,j} + (\epsilon_r^k)_{i,j-1} + (\epsilon_r^k)_{i,j+1} + (\epsilon_r^k)_{i+1,j}}{4}$$

iteratively for $k = 0, 1, 2, \dots$ until the iterations stagnate (at $k \approx 200$). The resulting values of ϵ_r are then interpolated onto the coarser meshes used in simulations. Similar homogenization procedures are also employed in FDTD codes, such as MEEP [41].

Table 1: The residual norm $\|r_m(T)\|$ (as defined by (14)) for different values of γ with resolution 16 and $\omega = 1$ and $m = 400$ iterations. The * sign means that some spurious eigenvalues have been detected and corrected, ** means that the value of γ is unacceptable as there are too many or too large spurious eigenvalues.

$\frac{\gamma}{T}$	residual norm
0.1*	1.63×10^0
0.05	1.60×10^0
0.025*	1.47×10^0
0.01	1.54×10^0
0.005	1.36×10^0
0.0025	1.39×10^0
0.001*	1.10×10^0
0.0005*	9.15×10^{-1}
0.00025**	7.60×10^{-5}

The matrix H_m produced by the regular Krylov method is a Galerkin projection of the matrix A , which means that $H_m = V_m^T A V_m$ and the field of values of H_m is a subset of the field of values of A . However, for the SaI Krylov method the matrix H_m results from the inverse SaI transformation (11) and therefore can have spurious eigenvalues. This can be especially pronounced for the matrices A with purely imaginary eigenvalues (or eigenvalues with very small real part), as is the case for our problem (4), see e.g. [7]. Indeed, if A has a purely imaginary eigenvalue $\lambda = iy$, $y \in \mathbb{R}$, then H_m can have eigenvalues approximating $\tilde{\lambda} = (1 + \gamma\lambda)^{-1} = (1 + i\gamma y)^{-1}$. The inverse SaI transformation of this approximate $\tilde{\lambda}$ may have a small real part of a negative sign, especially for large γy . In practice, this spurious eigenvalues with a small real part of the wrong sign can be replaced by the eigenvalues with zero real part. More precisely, once H_m is computed according to (11), we compute its Schur decomposition $H_m = QTQ^*$ and replace the small negative diagonal entries in T (if any) by zero. After that, we set $H_m = QTQ^*$ where T is now the corrected matrix.

We choose the parameter γ in the SaI Krylov subspace method by making cheap trial runs on a coarse mesh (in this case with resolution 16 points per unit length) and using the chosen γ for all the meshes [7]. This is possible because the SaI methods usually exhibit a mesh independent convergence [50, 25, 7]. We also look at the number and size of the spurious eigenvalues in the back SaI transformed matrix H_m . Typically we see that too many wrong eigenvalues can appear for large γ , so that γ should be chosen not too large. Table 1 shows the data of the test runs carried out to choose γ . Based on the data, for this particular case, we set $\gamma := 0.0005T = 0.25$.

To solve the projected ODE system (12), we use one of the standard Matlab's built-in stiff ODE solvers. It is important to use a stiff solver due to the PML boundary conditions and because the inverse SaI transformation (11) can yield large eigenvalues

Table 2: Performance of the ITR scheme

τ	relative error	CPU time
$\tau = \Delta x = 1/64$	4.12×10^{-1}	1.84×10^4
$\tau = \Delta x/2$	1.07×10^{-1}	3.74×10^4
$\tau = \Delta x/8$	6.33×10^{-3}	1.32×10^5

in H_m . In case a homogeneous projected ODE system is solved, i.e., $u'(t) = -H_m u(t)$, its solution is computed with the help of Matlab's matrix exponential function `expm` (see e.g. [30]).

4.2. Numerical results and discussion

We now compare the presented methods for the highest grid size possible on the PC we have, namely 64 grid points per unit length. On this mesh the size of the system (4) to be solved is $n = 4498307$. Since the spatial error is expected to be of order $(1/64)^2$, we should aim at the temporal error of the same order. Therefore, we set the residual tolerance in the Krylov methods to 10^{-4} . Recall that for the ITR method there is no residual available and, hence, its temporal error can not be easily controlled. Due to wave character of the problem, we expect that the time step τ in ITR should be at least of the same order as the spatial grid step, i.e., approximately $1/64$.

To check the actual accuracy achieved by the methods under comparison, we report the relative temporal error computed with respect to a reference solution $y_{\text{ref}}(t)$, i.e., $\|y(T) - y_{\text{ref}}(T)\|/\|y_{\text{ref}}(T)\|$. The reference solution is computed by the standard FDTD method ITR with a tiny time step size. Thus, this reference solution is expected to have the same spatial error as the methods to be compared. Hence, $y(T) - y_{\text{ref}}(T)$ can effectively be seen as the temporal error.

We start with examining the performance of the ITR scheme, see Table 2. Next, Table 3 shows the results for the Krylov subspace method (7)–(12),(15) with restarting in dimension, as presented in Section 3.3. In the table, we also show the results for the much coarser spatial mesh to demonstrate that the convergence of the method does not deteriorate as the mesh gets finer. Due to the independency of the method on the source time component $\alpha(t)$ (cf. Corollary 2), the CPU time required by the method for any other frequency from the range of interest is the CPU time needed for the projected ODE system, i.e., 6.21×10^3 s. Thus, for the second and subsequent frequencies, the gain we obtain with respect to the ITR scheme is a factor of $1.32 \times 10^5/6.21 \times 10^3 \approx 20$. A drawback of this method is that the used restart value $m_{\text{max}} = 400$ is very large, a larger restart value would hardly be possible due to computer memory limitations. For $m_{\text{max}} = 200$ no convergence is observed.

We now present the results for the two methods based on the splittings (16) and (19), respectively. In this methods, we are free to use both restarting in time and in space. By making cheap trial runs on coarse meshes, we choose the subinterval length for restart

Table 3: Results for the Krylov subspace method (7)–(12),(15) restarted in dimension every $m_{\max} = 400$ Krylov steps.

resolution	#restarts	residual norm	relative relative	total CPU time	CPU time for projected ODE
16	14	4.88×10^{-5}	–	2334.5	1252.0
64	12	1.53×10^{-5}	5.76×10^{-3}	3.09×10^4	6.21×10^3

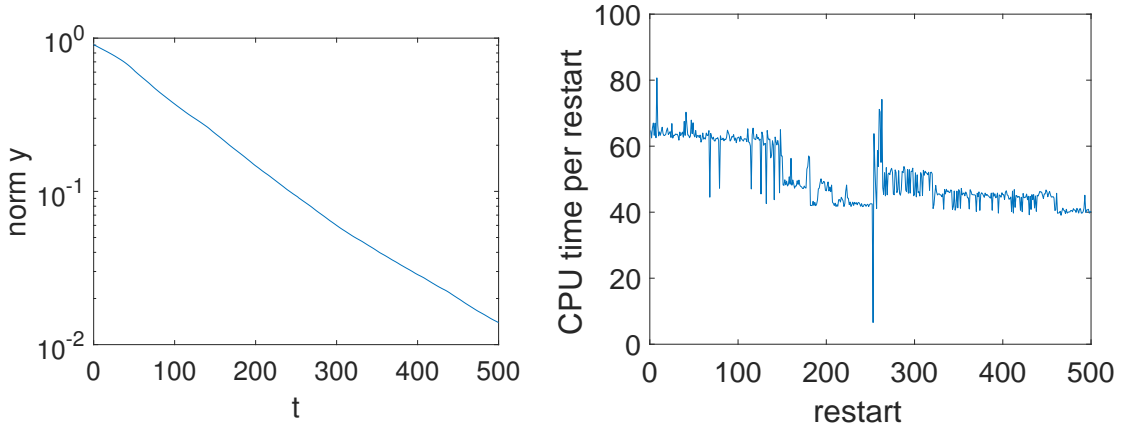


Figure 4: Left plot: $\|\hat{y}(t)\|$ versus t . Right plot: corresponding CPU times versus restarts in time.

in time to be 1. After that, the parameter γ is chosen as explained above, resulting in the value $\gamma = 0.01$. With these parameters, the Krylov subspace dimension has not exceeded 25 throughout restarts.

The results are given in Table 4. First of all, we demonstrate there that the time-periodic asymptotic solution $\tilde{y}(t)$ is a good approximation to the solution $y(t)$, it is even more accurate than ITR with the time step $\tau = \Delta x$. However, the accuracy of this solution is not of the order of the spatial error, which may not be enough. Comparing the results for the methods based on the splittings (16) and (19), we see that splitting (16) outperforms the other splitting. For both splittings a homogeneous problem of the type (17) has to be solved. The difference in performance is because the Krylov subspace method significantly profits from the fact that $\hat{y}(t)$ gets smaller in norm as time grows. Indeed, a small in norm initial value means a small initial residual (cf. (5),(6) with $g = 0$ and a small in norm v) and, hence, less steps to satisfy the required tolerance, see Figure 4. For the same reason, combination of this splitting with (18) turns out to be successful as well.

As shown, the method based on the splitting of the time-periodic asymptotic solution seems very promising: a significant gain factor (~ 13) with respect to the ITR method is achieved without utilizing a lot of memory.

Table 4: The performance of the two Krylov subspace solvers from Section 3.4.1

method	relative error	CPU time
time-periodic asymptotic solution $\tilde{y}(t)$	1.60×10^{-2}	4.95×10^1
splitting $\tilde{y}(t) + \hat{y}(t)$, cf. (16)	6.39×10^{-3}	2.53×10^4
splitting $\tilde{y}(t) + \hat{y}(t)$, next $\omega_{\text{next}} = \omega + 0.001$	–	9.75×10^3
splitting $w_1(t) + w_2(t)$, cf. (19)	7.08×10^{-3}	4.01×10^4

Table 5: Results for the most promising Krylov subspace methods and for the reference method ITR (gathered from Tables 2–4)

Method	Error	CPU time	Gain factor	Notes
ITR, $\tau = \Delta x/8$	6.33×10^{-3}	1.32×10^5	1	reference method
Krylov, splitting (16)	6.39×10^{-3}	2.53×10^4	5.22	
Krylov, splitting (16), ω_{next}	–	9.75×10^3	13.52	$\omega - \omega_{\text{next}} = 0.001$
Krylov, restarts in dimension	5.76×10^{-3}	3.09×10^4	4.27	high memory
Krylov, restarts in dimension, ω_{next}	–	6.21×10^3	21.26	requirements

Finally, in Table 5 we collect the results for the most promising methods and for the reference method ITR (run with the time step providing the required time accuracy $O(\Delta x)^2$). As shown for a single frequency, the Krylov subspace method based on the time-periodic asymptotic splitting is the fastest and provides a gain factor of 5.2 with respect to the reference method. At other frequencies, its gain factor of 13.5 is lower than the gain factor of the Krylov subspace method with restarting in dimension (21.3).

5. Conclusions

Standard Krylov subspace methods turn out to be inefficient in solving multi-frequency optical response from a scattering medium due to the growth of Krylov dimension. We overcome this inefficiency through two restarting strategies to restrict the Krylov dimension. The first approach is to restart in time, i.e., to use Krylov subspace methods on successive shorter subintervals. In this approach the invariance of the Krylov subspace on the time component $\alpha(t)$ is lost and we would need to use a block Krylov subspace. This approach is worked out and demonstrated to be inefficient in [29] due to the growth of the block size.

The other restarting approach we consider is the residual based restarting in Krylov dimension. This approach is shown to lead to a method where the large scale part of the computational work does not depend on the time component $\alpha(t)$. As numerical

experiments demonstrate, the new method works successfully only for very large Krylov dimensions. In the tests, this method appears to be the fastest, at the cost of high memory consumption.

To avoid the high memory requirements, we consider two other approaches based on the splitting. In the first one, the solution is split into an easy-to-compute time-periodic asymptotic part and the remaining part which decays with time. The Krylov subspace methods are demonstrated to be able to compute this decaying component very efficiently, thus providing a rigorous numerical solution to the whole problem. In the second approach, the periodicity of the source term is exploited. The problem is solved successfully on time subintervals and, on each subinterval, it is split into a homogeneous ODE system (i.e., with zero source term) and an inhomogeneous ODE whose solution is the same for all subintervals. The first, time-periodic asymptotic splitting appears to be more efficient and works well for multiple frequencies.

Thus, Krylov subspace exponential integrators seem to be a promising computational tool for modeling multi-frequency optical response with monochromatic sources.

- [1] M. Afanasjew, M. Eiermann, O. G. Ernst, and S. Güttel. Implementation of a restarted Krylov subspace method for the evaluation of matrix functions. *Linear Algebra Appl.*, 429:2293–2314, 2008.
- [2] E. Akkermans and G. Montambaux. *Mesoscopic physics of electrons and photons*. Cambridge university press, 2007.
- [3] A. H. Al-Mohy and N. J. Higham. Computing the action of the matrix exponential, with an application to exponential integrators. *SIAM J. Sci. Comput.*, 33(2):488–511, 2011. <http://dx.doi.org/10.1137/100788860>.
- [4] J. Bertolotti, E. G. van Putten, C. Blum, A. Lagendijk, W. L. Vos, and A. P. Mosk. Non-invasive imaging through opaque scattering layers. *Nature*, 491(7423):232–234, 2012.
- [5] R.-U. Börner, O. G. Ernst, and S. Güttel. Three-dimensional transient electromagnetic modelling using rational Krylov methods. *Geophysical Journal International*, 202(3):2025–2043, 2015.
- [6] M. A. Botchev. A block Krylov subspace time-exact solution method for linear ordinary differential equation systems. *Numer. Linear Algebra Appl.*, 20(4):557–574, 2013. <http://dx.doi.org/10.1002/nla.1865>.
- [7] M. A. Botchev. Krylov subspace exponential time domain solution of Maxwell’s equations in photonic crystal modeling. *J. Comput. Appl. Math.*, 293:24–30, 2016. <http://dx.doi.org/10.1016/j.cam.2015.04.022>.
- [8] M. A. Botchev, V. Grimm, and M. Hochbruck. Residual, restarting and Richardson iteration for the matrix exponential. *SIAM J. Sci. Comput.*, 35(3):A1376–A1397, 2013. <http://dx.doi.org/10.1137/110820191>.

- [9] M. A. Botchev and J. G. Verwer. Numerical integration of damped Maxwell equations. *SIAM J. Sci. Comput.*, 31(2):1322–1346, 2009. <http://dx.doi.org/10.1137/08072108X>.
- [10] M. Caliari and A. Ostermann. Implementation of exponential Rosenbrock-type integrators. *Appl. Numer. Math.*, 59(3-4):568–581, 2009.
- [11] E. Celledoni and I. Moret. A Krylov projection method for systems of ODEs. *Appl. Numer. Math.*, 24(2-3):365–378, 1997.
- [12] W. Chew, E. Michielssen, J. M. Song, and J. M. Jin, editors. *Fast and Efficient Algorithms in Computational Electromagnetics*. Artech House, Inc., Norwood, MA, USA, 2001.
- [13] T. A. Davis. Algorithm 832: UMFPACK V4.3—an unsymmetric-pattern multi-frontal method. *ACM Trans. Math. Software*, 30(2):196–199, 2004.
- [14] T. A. Davis. A column pre-ordering strategy for the unsymmetric-pattern multi-frontal method. *ACM Trans. Math. Software*, 30(2):167–195, 2004.
- [15] H. De Raedt, K. Michielssen, J. S. Kole, and M. T. Figge. One-step finite-difference time-domain algorithm to solve the Maxwell equations. *Phys. Rev. E*, 67:056706, 2003.
- [16] A. Dogariu and R. Carminati. Electromagnetic field correlations in three-dimensional speckles. *Physics Reports*, 559:1–29, 2015.
- [17] V. Druskin and R. Remis. A Krylov stability-corrected coordinate-stretching method to simulate wave propagation in unbounded domains. *SIAM Journal on Scientific Computing*, 35(2):B376–B400, 2013.
- [18] V. L. Druskin, A. Greenbaum, and L. A. Knizhnerman. Using nonorthogonal Lanczos vectors in the computation of matrix functions. *SIAM J. Sci. Comput.*, 19(1):38–54, 1998.
- [19] V. L. Druskin and L. A. Knizhnerman. Extended Krylov subspaces: approximation of the matrix square root and related functions. *SIAM J. Matrix Anal. Appl.*, 19(3):755–771, 1998.
- [20] I. S. Duff, A. M. Erisman, and J. K. Reid. *Direct methods for sparse matrices*. Oxford University Press, 2017.
- [21] M. Eiermann, O. G. Ernst, and S. Güttel. Deflated restarting for matrix functions. *SIAM J. Matrix Anal. Appl.*, 32(2):621–641, 2011.
- [22] I. Freund, M. Rosenbluh, and S. Feng. Memory effects in propagation of optical waves through disordered media. *Physical review letters*, 61(20):2328, 1988.

- [23] A. Frommer, K. Lund, and D. B. Szyld. Block krylov subspace methods for computing functions of matrices applied to multiple vectors. Report 17-03-21, Department of Mathematics, Temple University, March 2017. www.math.temple.edu/~szyld.
- [24] M. J. Gander and S. Güttel. Paraexp: A parallel integrator for linear initial-value problems. *SIAM Journal on Scientific Computing*, 35(2):C123–C142, 2013.
- [25] T. Gökler and V. Grimm. Uniform approximation of φ -functions in exponential integrators by a rational Krylov subspace method with simple poles. *SIAM Journal on Matrix Analysis and Applications*, 35(4):1467–1489, 2014. <http://dx.doi.org/10.1137/140964655>.
- [26] S. A. Goorden, M. Horstmann, A. P. Mosk, B. Škorić, and P. W. H. Pinkse. Quantum-secure authentication of a physical unclonable key. *Optica*, 1(6):421–424, 2014.
- [27] S. Güttel. *Rational Krylov Methods for Operator Functions*. PhD thesis, Technischen Universität Bergakademie Freiberg, March 2010. www.guettel.com.
- [28] S. Güttel, A. Frommer, and M. Schweitzer. Efficient and stable Arnoldi restarts for matrix functions based on quadrature. *SIAM J. Matrix Anal. Appl*, 35(2):661–683, 2014.
- [29] A. M. Hanse. Krylov subspace time domain computations of monochromatic sources for multi-frequency optical response. MSc Thesis, Department of Applied Mathematics, University of Twente, April 2017. <http://essay.utwente.nl/72241/>.
- [30] N. J. Higham. *Functions of Matrices: Theory and Computation*. Society for Industrial and Applied Mathematics, Philadelphia, PA, USA, 2008.
- [31] M. Hochbruck and A. Ostermann. Exponential integrators. *Acta Numer.*, 19:209–286, 2010.
- [32] M. Hochbruck, T. Pažur, A. Schulz, E. Thawinan, and C. Wieners. Efficient time integration for discontinuous Galerkin approximations of linear wave equations. *ZAMM*, 95(3):237–259, 2015.
- [33] W. Hundsdorfer and J. G. Verwer. *Numerical Solution of Time-Dependent Advection-Diffusion-Reaction Equations*. Springer Verlag, 2003.
- [34] S. G. Johnson. Notes on perfectly matched layers (PMLs). math.mit.edu/~stevenj/18.369/pml.pdf, March 2010.
- [35] O. Katz, P. Heidmann, M. Fink, and S. Gigan. Non-invasive single-shot imaging through scattering layers and around corners via speckle correlations. *Nature Photonics*, 8(10):784–790, 2014.

- [36] L. Knizhnerman and V. Simoncini. A new investigation of the extended Krylov subspace method for matrix function evaluations. *Numer. Linear Algebra Appl.*, 17(4):615–638, 2010.
- [37] C. B. Moler and C. F. Van Loan. Nineteen dubious ways to compute the exponential of a matrix, twenty-five years later. *SIAM Rev.*, 45(1):3–49, 2003.
- [38] I. Moret and P. Novati. RD rational approximations of the matrix exponential. *BIT*, 44:595–615, 2004.
- [39] M. Mounaix, D. Andreoli, H. Defienne, G. Volpe, O. Katz, S. Grésillon, and S. Gigan. Spatiotemporal coherent control of light through a multiple scattering medium with the multispectral transmission matrix. *Phys. Rev. Lett.*, 116:253901, Jun 2016.
- [40] J. Niehoff. *Projektionsverfahren zur Approximation von Matrixfunktionen mit Anwendungen auf die Implementierung exponentieller Integrioren*. PhD thesis, Mathematisch-Naturwissenschaftlichen Fakultät der Heinrich-Heine-Universität Düsseldorf, December 2006.
- [41] A. F. Oskooi, C. Kottke, and S. G. Johnson. Accurate finite-difference time-domain simulation of anisotropic media by subpixel smoothing. *Optics letters*, 34(18):2778–2780, 2009.
- [42] B. Redding, S. F. Liew, R. Sarma, and H. Cao. Compact spectrometer based on a disordered photonic chip. *Nature Photonics*, 7(9):746–751, 2013.
- [43] Y. Saad. *Iterative Methods for Sparse Linear Systems*. SIAM, 2d edition, 2003. Available from <http://www-users.cs.umn.edu/~saad/books.html>.
- [44] D. Sármany, M. A. Botchev, and J. J. W. van der Vegt. Time-integration methods for finite element discretisations of the second-order Maxwell equation. *Computers & Mathematics with Applications*, 65(3):528–543, 2013.
- [45] T. Schmelzer and L. N. Trefethen. Evaluating matrix functions for exponential integrators via Carathéodory-Fejér approximation and contour integrals. *Electron. Trans. Numer. Anal.*, 29:1–18, 2007/08.
- [46] R. B. Sidje. EXPOKIT. A software package for computing matrix exponentials. *ACM Trans. Math. Softw.*, 24(1):130–156, 1998. www.maths.uq.edu.au/expokit/.
- [47] A. Taflove and S. C. Hagness. *Computational electrodynamics: the finite-difference time-domain method*. Artech House Inc., Boston, MA, third edition, 2005.
- [48] H. Tal-Ezer. Spectral methods in time for parabolic problems. *SIAM J. Numer. Anal.*, 26(1):1–11, 1989.
- [49] H. Tal-Ezer. On restart and error estimation for Krylov approximation of $w = f(A)v$. *SIAM J. Sci. Comput.*, 29(6):2426–2441, 2007.

- [50] J. van den Eshof and M. Hochbruck. Preconditioning Lanczos approximations to the matrix exponential. *SIAM J. Sci. Comput.*, 27(4):1438–1457, 2006.
- [51] H. A. van der Vorst. *Iterative Krylov methods for large linear systems*. Cambridge University Press, 2003.
- [52] M. C. W. v. van Rossum and T. M. Nieuwenhuizen. Multiple scattering of classical waves: microscopy, mesoscopy, and diffusion. *Reviews of Modern Physics*, 71(1):313, 1999.
- [53] J. G. Verwer and M. A. Botchev. Unconditionally stable integration of Maxwell’s equations. *Linear Algebra and its Applications*, 431(3–4):300–317, 2009.
- [54] K. S. Yee. Numerical solution of initial boundary value problems involving Maxwells equations in isotropic media. *IEEE Trans. Antennas Propagat.*, 14(3):302–307, March 1966.
- [55] H. Yilmaz, E. G. van Putten, J. Bertolotti, A. Lagendijk, W. L. Vos, and A. P. Mosk. Speckle correlation resolution enhancement of wide-field fluorescence imaging. *Optica*, 2(5):424–429, 2015.